(Received 20 October 2023, Accepted 20 November 2023, Scheduled 1 December 2023)

A Small Size Wideband M-Shaped Polygonal Slot Antenna for X-Band Satellite Applications

Mostafa M. Rabie[1, 2, *], Mohamed S. El-Gendy[3], Angie R. El Damak[2], Fawzy Ibrahim[4], and Hadia El-Henawy[2]

[1] *Electrical and Electronics Engineering, Coventry University, Cairo, Egypt*
[2] *Electronics and Communications Engineering Department, Ain Shams University, Cairo, Egypt*
[3] *Electronics Research Institute, Cairo, Egypt*
[4] *Egyptian Academy for Engineering and Advanced Technology, Cairo, Egypt*

ABSTRACT: This paper presents a small size M-shaped polygonal slot antenna for X-band satellite telemetry and Synthetic Aperture Radar (SAR) applications. The proposed antenna has been designed on a Roger RT-Duroid 5880 substrate. The reflection coefficient $|S_{11}|$ of the proposed antenna covers the whole X-band from 6.63 GHz to 12.566 GHz. The proposed antenna is circularly polarized with axial ratio (AR) bandwidth that extends from 7.76 GHz to 8.58 GHz. The proposed antenna provides a simultaneous dual circular polarizations (RHCP and LHCP). The gain of the proposed antenna varies between 6.6 dBi and 9.4 dBi. The proposed antenna realizes an efficiency of 92%. The overall size of the proposed antenna is $17 \times 16 \times 0.508\,\text{mm}^3$ $(0.56\lambda_0 \times 0.53\lambda_0 \times 0.016\lambda_0)$. Therefore, it is suitable to be employed in satellite telemetry application from 7.9 GHz to 8.4 GHz especially for CubeSats that have limited surface area. Apart from that, this antenna finds its applications in SAR on small satellites from 9 GHz to 10 GHz, military, and RFID tag (tracking equipment). It has been observed that the measurement results match the simulated ones. The proposed antenna design can be practically employed for the previously mentioned applications.

1. INTRODUCTION

The use of X-band technology has been pivotal in enabling high-speed data transmission, large bandwidth, and short-range communication for a wide range of applications. One of the most significant applications of the antenna operating in X-band is satellite telemetry, where it is used for communication between the satellite and the ground station. In particular, the X-band antenna used for telemetry applications is operating in the frequency range from 7.9 GHz to 8.4 GHz and with circularly polarized performance to ensure reliable communication [1–3]. Another application of the X-band antenna is in Synthetic Aperture Radar (SAR) on small satellites. SAR is a radar imaging technique that uses the motion of the radar antenna over a target to provide high-resolution images. X-band antenna is used in SAR applications in the frequency range from 9 GHz to 10 GHz, where circular polarization is not required [4, 5]. Additionally, X-band antenna is used in military applications for communication and surveillance purposes [6]. Finally, X-band antenna is also used in RFID tags for tracking equipment at a frequency of 10 GHz, where circular polarization is not required [7]. Despite the significant advancements made in X-band antenna design, X-band antennas that can cater to diverse applications continues to pose a major challenge for researchers. The need for compact, lightweight, and easily integrable antennas in modern communication systems has led to a growing interest in the development of such antennas. Planar antennas have emerged as a popular choice due to their low cost, ease of fabrication, low profile, and compatibility with circuit technology. They have been widely used in high-performance satellites, CubeSats, and wireless communication devices [8–10]. However, these antennas suffer from major drawbacks such as low bandwidth, low power handling capacity, and low gain, which significantly limit their performance [11]. To overcome these limitations and achieve wide bandwidth and acceptable gain with very small antenna sizes, researchers have focused on developing new antenna designs. The development of X-band antennas that meet the requirements of different applications is considered an attractive and challenging area of research, and many researchers have shown considerable interest in this field [1–4, 12, 13]. Several antenna designs operating in the X-band satellite telemetry and SAR applications were investigated. The first antenna in [1] is a compact telemetry antenna with simultaneous dual circular polarizations, covering a bandwidth from 8.025 GHz to 8.4 GHz, with a 3 dB axial ratio bandwidth of 370 MHz and a maximum gain of 5 dBi. The antenna size is 238 mm $(6.52\lambda_0)$ in diameter and 185 mm $(5.13\lambda_0)$ in height, which is considered a large size. The second antenna in [2] is a high gain compact circularly polarized superstrate antenna for CubeSat applications, with a bandwidth of 8–9.7 GHz, a 3 dB axial ratio bandwidth of 580 MHz, and a maximum gain of 14 dBi. The antenna size is $62 \times 62 \times 22\,\text{mm}^3$ $(1.77\lambda_0 \times 1.77\lambda_0 \times 0.63\lambda_0)$. The third antenna in [3] is a telemetry circularly polarized antenna for CubeSats, with a bandwidth extending from 8 GHz to 8.4 GHz, a 3 dB axial ratio bandwidth of 400 MHz, and a maximum gain of 5 dBi. The antenna size is $100 \times 100 \times 15\,\text{mm}^3$ $(2.74\lambda_0 \times 2.74\lambda_0 \times 0.41\lambda_0)$. The fourth an-

* Corresponding author: Mostafa Mahmoud Rabie (ad8259@coventry.ac.uk).

tenna in [4] is a broadband substrate integrated waveguide antenna for X-band SAR application, with a bandwidth extending from 9.4 GHz to 10.5 GHz. The antenna is not circularly polarized, and it achieves a maximum gain of 9 dBi. The antenna size is $59 \times 14 \times 0.76\,\text{mm}^3$ ($1.96\lambda_0 \times 0.46\lambda_0 \times 0.025\lambda_0$). The fifth antenna in [5] is a broadband planar antenna for X-band SAR onboard small satellites, with a bandwidth extending from 9.01 GHz to 10.2 GHz. The antenna is not circularly polarized, and it achieves a maximum gain of 8 dBi. The antenna size is $14 \times 14 \times 3.986\,\text{mm}^3$ ($0.45\lambda_0 \times 0.45\lambda_0 \times 0.126\lambda_0$).

This paper focuses on designing a wideband antenna operating in the X-band for both telemetry and SAR applications. The antenna is designed to achieve a high gain with a small size compared to the previously mentioned designs. The idea of this paper is based on fractal antennas [14]. Fractals have been used commercially in antennas since the 2010s [14]. The main advantages of fractal antennas are wide bandwidth, high gain, and small area [14]. The high gain with small size results from constructive interference with multiple current maxima, afforded by the electrically long structure in a small area [14]. In this paper, the idea was based on increasing the effective slot length of a rectangular slot antenna in a way to achieve the required bandwidth with a miniaturized overall antenna size. Asymmetry in the slot shape is also introduced during the process to achieve circular polarization [15, 16]. This can be achieved by selecting a number of arbitrary points in the rectangle slot and then performing parametric analysis on their position in the x and y directions until attaining the effective length that achieves the required bandwidth. Also, reaching an asymmetric shape will provide the required axial ratio (AR) bandwidth. This study presents a simple and effective technique based on an embedded structure for the design of a compact wideband circularly polarized slot antenna. The proposed design consists of an M-shaped polygonal slot with an embedded M-shaped polygonal island. A microstrip feedline ended with a trapezoidal shaped stub is used for excitation of the proposed M-shaped polygonal slot antenna. This paper is organized as follows. The rectangular slot antenna design is introduced in Section 2. M-shaped polygonal slot realization steps and parametric analysis are performed in Section 3. The proposed design is given in Section 4. Final assessment and comparison with recent X-band antenna designs are introduced in Section 5. Result analysis and conclusions are given in Section 6.

2. RECTANGULAR SLOT ANTENNA DESIGN

2.1. Rectangular Slot Antenna with Rectangular Feedline (RSA-RF)

The rectangular slot antenna consists of three layers: the top layer where the slot takes place, the bottom layer where the feeding line exists, and the third layer being Rogers RT-Duroid 5880 with dielectric constant, ε_r of 2.2, low loss tangent $\tan(\delta) = 0.0009$, and thickness, $h = 0.508\,\text{mm}$. The first step of the antenna design procedure is cutting a rectangular slot in the top layer with dimensions $PW \times PL_1$ as shown in Figure 1(a). The dimensions of the rectangular slot are calculated at resonance frequency, $f_r = 8.15\,\text{GHz}$, as follows [17–20]:

$$PW \cong \frac{n\lambda_g}{2} = \frac{nC}{2f\sqrt{\varepsilon_{reff}}} \tag{1}$$

$$PL_1 < \frac{PW}{2} \tag{2}$$

where n is an odd integer ($n = 1, 3, 5...$), c the speed of light ($c = 3 \times 10^8$), λ_g the guided wavelength, and ε_{reff} the effective dielectric constant. Increasing the value of n increases the gain of the antenna [20]. The overall dimensions of the conventional antenna were calculated to be slightly greater than PW as follows [17, 19]:

$$L \cong W > PW \tag{3}$$

where L and W are the overall length and width of the antenna, respectively as shown in Figure 1(a). The slot antenna is fed by a microstrip feedline at the bottom layer as shown in Figure 1(b). The length and width of the feedline are L_f and W_f, respectively. The feedline is placed in the middle of the antenna at a distance of F_L from the left edge of the bottom layer as shown in Figure 1(b). The rectangular slot antenna with a rectangular feedline is simulated using CST studio suite. The value of 'n' is selected to be equal to 3 for gain increasing. Also, the reason behind selecting a slot width of $\frac{3\lambda_g}{2}$ instead of $\frac{\lambda_g}{2}$ is to increase the width of the slot, PW, and accordingly increase the length of the slot, PL_1, to increase the whole size of the aperture, $(PW \times PL_1)$, in order to insert the embedded island inside the slot as discussed later in step 2. Figure 2(a) shows the reflection coefficient $|S_{11}|$ of the RSA-RF at $PW \cong \frac{\lambda_g}{2}$ and $\frac{3\lambda_g}{2}$, indicating that the RSA-RF resonates at the same frequency ($f_r = 8.15\,\text{GHz}$) with the same bandwidth for both values of PW. Figure 2(b) shows the gain of the RSA-RF at $PW \cong \frac{\lambda_g}{2}$ and $\frac{3\lambda_g}{2}$, with the maximum gain of 3 dBi and 8.8 dBi, respectively. This indicates a significant increase in gain at $PW = \frac{3\lambda_g}{2}$ with a 5.8 dBi gain improvement. The dimensions of the RSA-RF for $PW \cong \frac{\lambda_g}{2}$ and $\frac{3\lambda_g}{2}$ are given in Table 1. The reflection coefficient $|S_{11}|$ of the RSA-RF at this step is shown in Figure 7. The bandwidth is 670 MHz extending from 7.8 GHz to 8.47 GHz. The overall size ($L \times W$) of the RSA-RF is $51.2 \times 49\,\text{mm}^2$. The optimized dimensions of the RSA-RF at this step are given in Table 2. In the upcoming subsection, a rectangular embedded island would be placed within the rectangular slot to improve the bandwidth and size.

2.2. Rectangular Slot with Embedded Island and Rectangular Feedline (RSEI-RF)

An embedded island is placed inside the rectangular slot as shown in Figure 3(a) for reflection coefficient $|S_{11}|$, bandwidth, and size improvement [21–24]. The slot antenna is fed by a microstrip feedline at the bottom layer as shown in Figure 3(b). The antenna is then simulated with a rectangular feedline and embedded island. The embedded island is a downscaled version of the slot multiplied by SF, where SF is the scaling factor. The length and width of the embedded island are PL_1' and PW', respectively, and are given as follows:

$$PL_1' = SF \times PL_1 \tag{4}$$

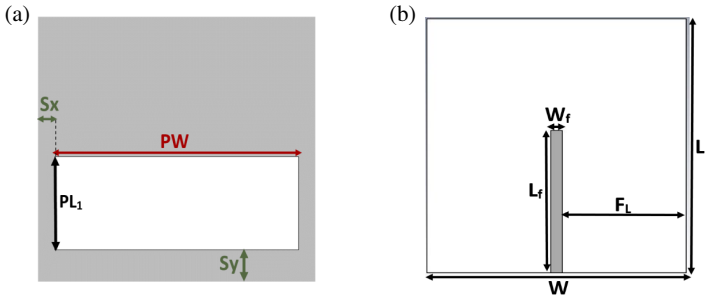

FIGURE 1. Rectangular slot antenna with rectangular feedline (RSA-RF): (a) Front view, (b) back view.

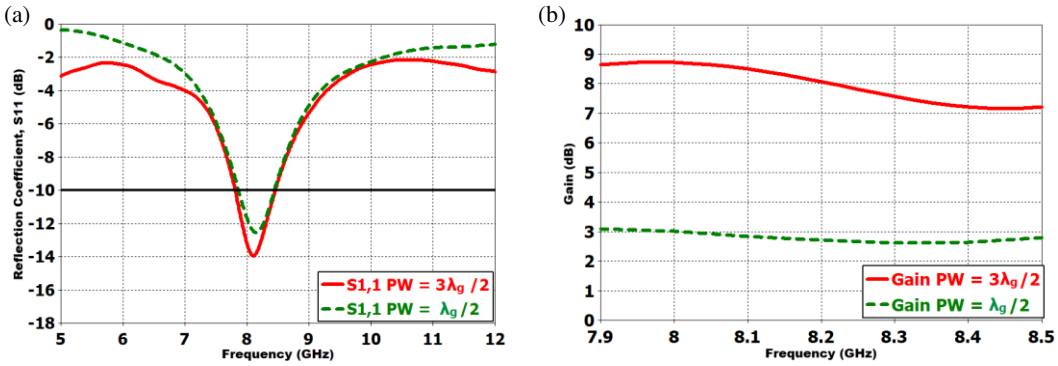

FIGURE 2. Simulated antenna parameters of the RSA-RF at $PW \cong \frac{\lambda_g}{2}$ and $\frac{3\lambda_g}{2}$: (a) Reflection coefficient $|S_{11}|$, (b) gain.

TABLE 1. Dimensions of RSA-RF at $PW \cong \frac{\lambda_g}{2}$ and $\frac{3\lambda_g}{2}$.

	RSA-RF at $PW \cong \frac{\lambda_g}{2}$	RSA-RF at $PW \cong \frac{3\lambda_g}{2}$
Parameter	**Value (mm)**	**Value (mm)**
PL_1	3	18
PW	14	43
Sx	2.5	3
Sy	4.4	6.3
L	18	51.2
W	17	49
W_f	1.53	1.53
L_f	6	29
F_L	7.7	23.7

$$PW' = SF \times PW \tag{5}$$

Parametric analysis is performed on the scaling factor, SF. The RSEI-RF is simulated at different values of SF. Figure 4 shows that the reflection coefficient $|S_{11}|$ of the RSEI-RF at SF equals 0.38, 0.58, and 0.68. The selected value of SF is 0.58 where it achieves the required reflection coefficient $|S_{11}|$ and bandwidth. Parametric analysis is then performed on the position of the island Sx_2 and Sy_2. The RSEI-RF is simulated at different values of Sx_2 and Sy_2 as shown in Figures 5(a) and (b). Figure 5(a) shows the reflection coefficient $|S_{11}|$ of the RSEI-RF at Sx_2 which equals 2.22 mm, 3.22 mm, and 6.22 mm. The Sx_2 value of 6.22 mm is selected to realize the required reflection coefficient $|S_{11}|$ and bandwidth. Figure 5(b) shows the reflection coefficient $|S_{11}|$ of the RSEI-RF at Sy_2 equals 0.68 mm, 1.03 mm, and 1.38 mm. The Sy_2 value of 0.68 mm is selected to realize the required reflection coefficient $|S_{11}|$ and bandwidth. The reflection coefficient $|S_{11}|$ at the selected values of SF, Sx_2 and Sy_2 is shown in Figure 7 to be compared to the RSA-RF. The bandwidth is 1.95 GHz extending from 6.56 GHz to 8.51 GHz. It is shown from Figure 7 that there is an improvement of 191% in the bandwidth compared to the RSA-RF in the previous step. The overall size ($L \times W$) of the RSEI-RF is $35.3 \times 33.8\,\text{mm}^2$. The overall size ($L \times W$) of the RSEI-RF is reduced by 52.5% compared to the RSA-RF in the previous step. The dimensions of the antenna are given in Table 2. Improvement in the bandwidth and size is clear compared to the RSA-RF in the previous step. In the upcoming subsection the microstrip feedline will be terminated with a trapezoidal stub which will show an improvement in bandwidth and size.

TABLE 2. Optimized dimensions of RSA-RF, RSEI-RF and RSEI-TS.

	RSA-RF	RSEI-RF	RSEI-TS
Parameter	**Value (mm)**	**Value (mm)**	**Value (mm)**
PL_1	18	12.35	11
PW	43	29.7	26.6
PL_1'	-	7.16	6.38
PW'	-	17.22	15.43
Sx	3	2.08	1.872
Sx_2	-	6.22	5.53
Sy	6.3	4.32	3.8
Sy_2	-	0.68	0.7
L_f	29	19.75	8
L_{tap}	-	-	7.6
W_f	1.53	1.53	1.53
W_{tap}	-	-	4.4
F_L	23.7	16.13	14.4
L	51.2	35.3	31.7
W	49	33.8	30.4

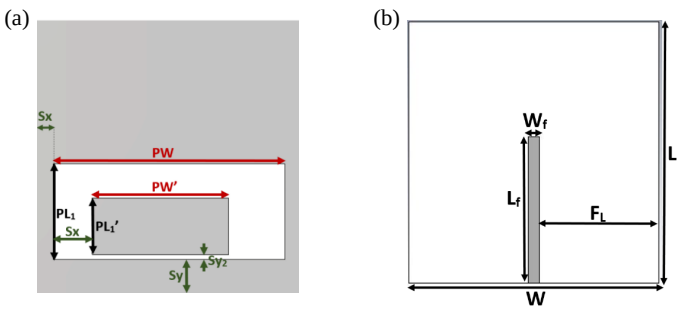

FIGURE 3. Rectangular slot with embedded island and rectangular feedline (RSEI-RF): (a) Front view, (b) back view.

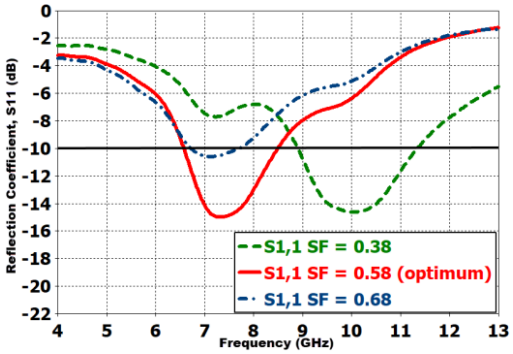

FIGURE 4. Simulated reflection coefficient $|S_{11}|$ of the RSEI-RF at different values of SF.

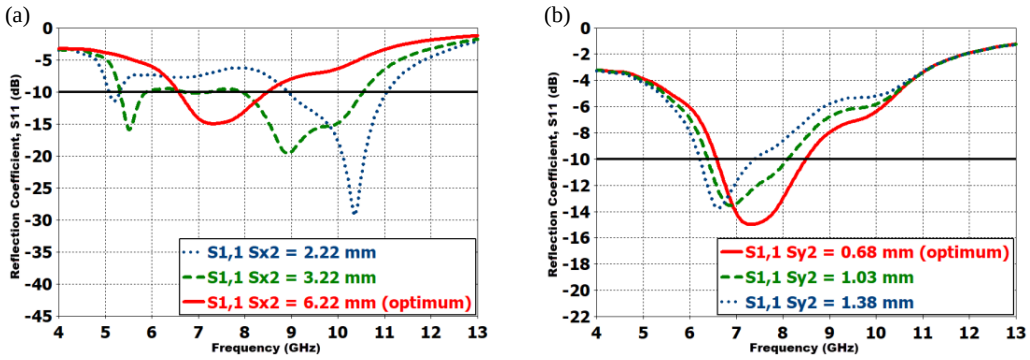

FIGURE 5. Simulated reflection coefficient $|S_{11}|$ of the RSEI-RF at different values of: (a) Sx_2, (b) Sy_2.

2.3. Rectangular Slot with Embedded Island and Trapezoidal Stub (RSEI-TS)

For further reduction in size and for extending bandwidth, the antenna is fed by a microstrip line ending with a trapezoidal stub in the bottom layer as shown in Figure 6(b) [23]. The trapezoidal stub at the end of the feedline has a length of L_{tap}. The trapezoidal stub beginning width is W_f and end width W_{tap}. The feedline is placed at a distance of F_L from the left side as show in Figure 6(b). The reflection coefficient $|S_{11}|$ is shown in Figure 7. The bandwidth is 2.65 GHz extending from 6.55 GHz to 9.2 GHz. It is shown from Figure 7 that there is an improvement of 35.9% in the bandwidth compared to the RSEI-RF in

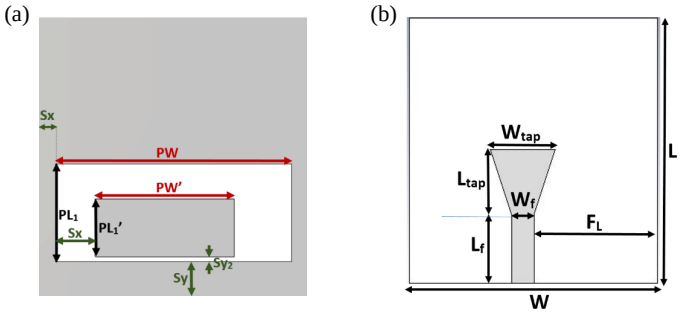

FIGURE 6. Rectangular slot with embedded island and trapezoidal stub (RSEI-TS): (a) Front view, (b) back view.

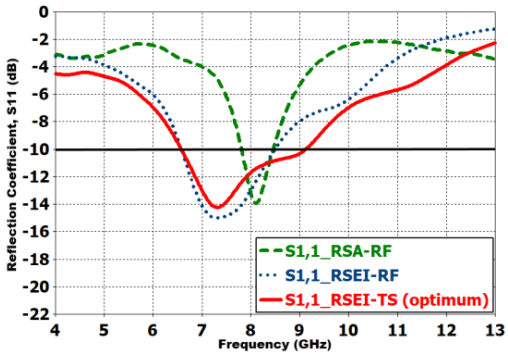

FIGURE 7. Simulated reflection coefficient $|S_{11}|$ of the RSA-RF, RSEI-RF and RSEI-TS.

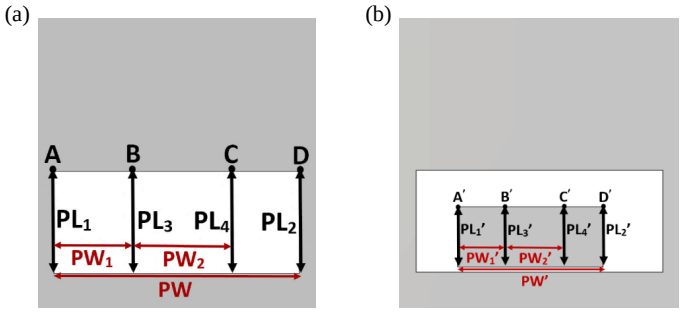

FIGURE 8. Dimensions of the RSEI-TS front view: (a) Slot dimensions, (b) island dimensions.

the previous step. The overall size ($L \times W$) of the RSEI-TS is $31.7 \times 30.4\,\text{mm}^2$. The overall size of the RSEI-TS is reduced by 19.3% compared to the RSEI-RF in the previous step. The dimensions of the antenna are given in Table 2. Improvement in the bandwidth and size is clear compared to the RSEI-RF in the previous step. In the upcoming section an M-shaped polygonal slot with embedded M-shaped polygonal island will be realized from the RSEI-TS and parametrically analyzed. The reason behind this is bandwidth increasing, achieving circular polarization for the telemetry application band (7.9 GHz–8.4 GHz) and for extra reduction in size.

3. M-SHAPED POLYGONAL SLOT REALIZATION STEPS AND PARAMETRIC ANALYSIS

For further reduction in the antenna size, bandwidth enhancements, and achieving circular polarization, the following technique is applied on the RSEI-TS to increase the effective length of the slot within a miniaturized overall surface area of the slot antenna. The technique is also used to introduce a symmetry in the slot shape to achieve circular polarization (axial ratio (AR) $<$ 3 dB) [15, 16]. The asymmetrical shape of the slot is a key factor in achieving circular polarization [15, 16, 19]. The asymmetrical slot is designed to have a nonuniform shape that creates a phase difference between the electric field components in the slot [15, 16, 19]. This phase difference results in the generation of a circularly polarized wave [15, 16, 19]. Four points A, B, C, and D are selected at the upper edge of the rectangular slot in the RSEI-TS as shown in Figure 8(a). The locations of the points in the x and y directions are attuned so that the required bandwidth, axial ratio (AR), and size can be achieved. The four points are used to control the effective length of the slot along with controlling the symmetry of the shape. Modifications in the heights of the points (PL_1, PL_2, PL_3 and PL_4), along with modifications in the distance between them (PW_1 and PW_2) as shown in Figure 8, will convert the slot shape into an M-shaped polygon. This idea is inspired by the idea of fractal antennas where large bandwidths and circular polarization can be achieved while maintaining a small size of the whole antenna [25, 14]. Although the incentive here is even having full control on the overall shape and dimensions without being restricted with a certain pattern of repetition. Any changes in the locations of A, B, C, and D will reflect on the locations of A′, B′, C′, and D′ so that the embedded island will always have the same shape of the slot with dimensions multiplied by the scaling factor, SF, as shown in Figure 8(b). The rectangular embedded island in Figure 8(b) has points' heights of (PL'_1, PL'_2, PL'_3, and PL'_4) with distances between the points of (PW'_1 and PW'_2) and are respectively given as follows:

$$PL'_n = SF \times PL_n; \quad n = 1, 2, 3, 4. \tag{6}$$

$$PW'_n = SF \times PW_n; \quad n = 1, 2. \tag{7}$$

A parametric study on the points' locations is performed until reaching the required bandwidth, axial ratio (AR), and size. Miniaturization of the overall size of the antenna is performed by changing the heights of the points which increases the effective length of the slot. Four steps took place involving a parametric study on PL_1, PL_2, PL_3, and PL_4.

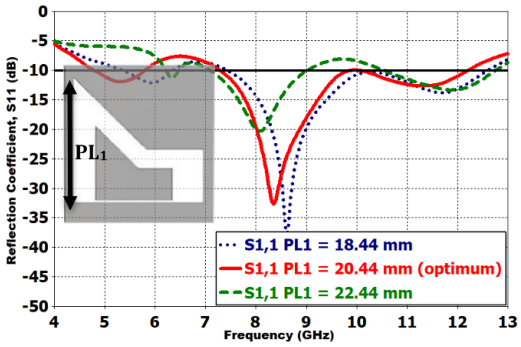

FIGURE 9. Simulated reflection coefficient $|S_{11}|$ of the RSEI-TS at different values of PL_1.

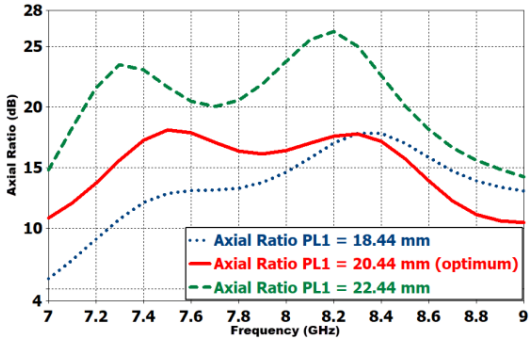

FIGURE 10. Simulated axial ratio (AR) of the RSEI-TSat different values of PL_1.

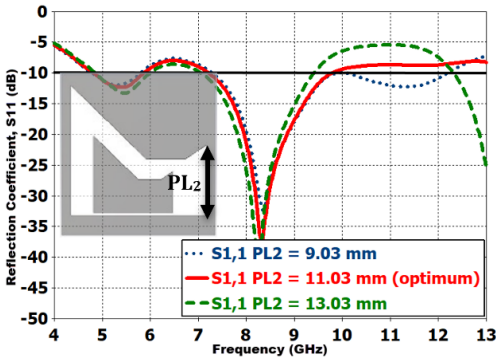

FIGURE 11. Simulated reflection coefficient $|S_{11}|$ of the RSEI-TS with updated value of PL_1 at different values of PL_2.

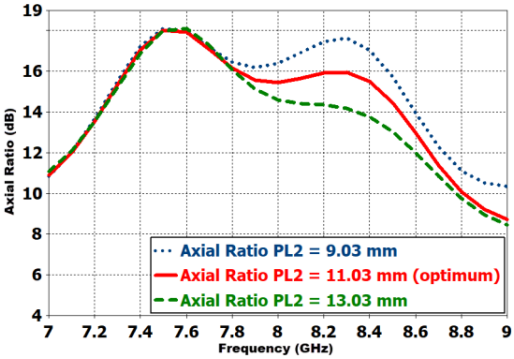

FIGURE 12. Simulated axial ratio (AR) of the RSEI-TS with updated value of PL_1 at different values of PL_2.

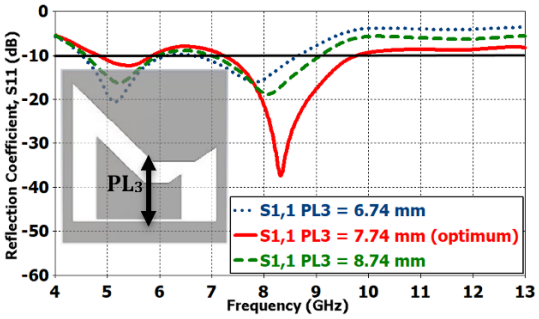

FIGURE 13. Simulated reflection coefficient $|S_{11}|$ of the RSEI-TS with updated value of PL_1 and PL_2 at different values of PL_3.

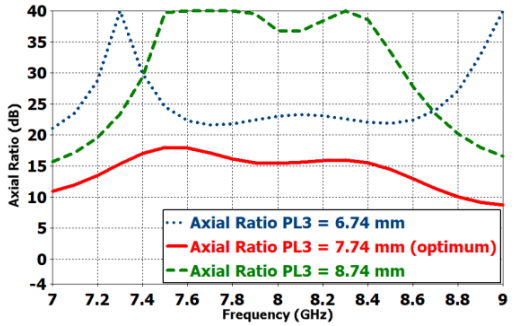

FIGURE 14. Simulated axial ratio (AR) of the RSEI-TS with updated values of PL_1 and PL_2 at different values of PL_3.

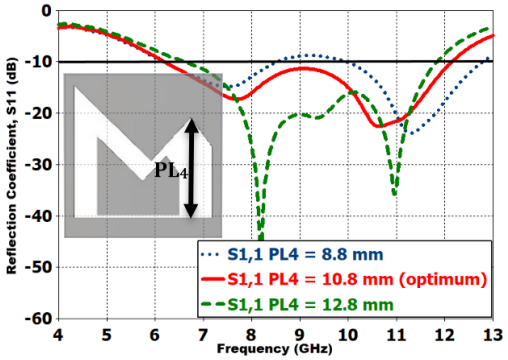

FIGURE 15. Simulated reflection coefficient $|S_{11}|$ of the RSEI-TS with updated values of PL_1, PL_2 and PL_3 at different values of PL_4.

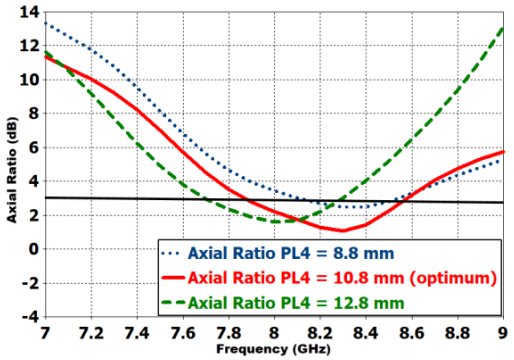

FIGURE 16. Simulated axial ratio (AR) of the RSEI-TS with updated values of PL_1, PL_2 and PL_3 at different values of PL_4.

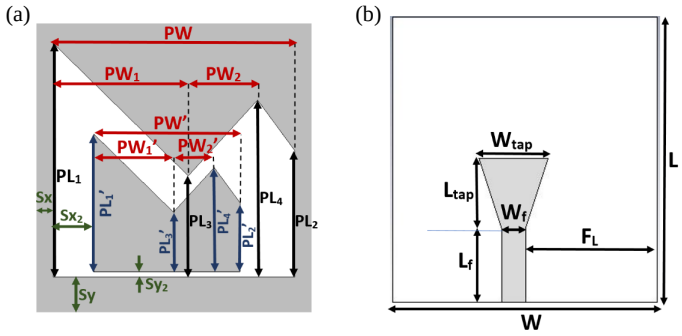

FIGURE 17. M-shaped polygonal slot antenna with embedded island: (a) Front view, (b) back view.

(a) (b)

FIGURE 18. Fabricated M-shaped polygonal slot antenna with the embedded island: (a) Front view, (b) back view.

FIGURE 19. Fabricated M-shaped polygonal slot antenna with the embedded island measurement in the anechoic chamber.

Increasing or decreasing the height of any of the four points will increase the overall slot length, lowering the operating frequency, and lowering the frequency range. Therefore, the desired bandwidth and 3-dB axial ratio bandwidth will be achieved but at a lower frequency range. To restore the antenna to the desired operating frequency and achieve the desired 3-dB axial ratio bandwidth, the frequency transformation technique in [26] is applied after altering any of the points' heights. This technique ensures that the frequency range and 3-dB axial ratio bandwidth are brought back to the desired range. Furthermore, employing the frequency transformation technique allows for a reduction in the overall size of the antenna. As all the dimensions decrease proportionally, the antenna's size is effectively decreased. The frequency transformation technique indicates that to move a certain operating band to a desired operating band all the dimensions of the antenna are multiplied by the (center frequency of the current band) divided by the (center frequency of the desired band). The frequency transformation equation is as follows:

$$L_{\text{new}} = L_{\text{old}} \times \frac{f_{\text{current}}}{f_{\text{desired}}} \tag{8}$$

where L_{old} represents any of the antenna dimensions after changing the height of one of the four points. L_{new} represents the new dimensions of the antenna after adjusting the operating band. f_{current} is the center frequency of the lowered frequency range due to altering any of the heights of the four points. f_{desired} is the center frequency of the desired frequency range.

3.1. Step 1: Studying the Effect of Length PL_1

In this step, parametric study is performed on PL_1. The RSEI-TS antenna shown in Figure 8 is simulated at different values of PL_1 while the other parameters are kept constant. The overall antenna size is reduced due to increasing the value of PL_1 which increases the effective length of the slot. Consequently, to maintain the same operating frequency band the overall antenna size is miniaturized. The overall antenna size ($L \times W$) is $25.3 \times 24.2\,\text{mm}^2$. The overall antenna size is reduced by 36.5% compared to the RSEI-TS. The dimensions of the antenna at this step are given in Table 3. The reflection coefficient $|S_{11}|$ and the axial ratio (AR) curves for different values of PL_1 are shown in Figure 9 and Figure 10, respectively. It is shown in Figure 9 that the bandwidth at $PL_1 = 18.44\,\text{mm}$, 20.44 mm, and 22.44 mm is 2.1 GHz, 3 GHz, and 2 GHz, respectively. $PL_1 = 20.44\,\text{mm}$ achieves the largest bandwidth with an improvement of 13.2% compared to the RSEI-TS. It is shown in Figure 10 that the axial ratio (AR) in the band (7.9 GHz–8.4 GHz) for the three values of PL_1 exceeds 3 dB. The axial ratio for $PL_1 = 18.44\,\text{mm}$, 20.44 mm, and 22.44 mm is in the range between (14 dB–18 dB), (16 dB–17 dB) and (22.5 dB–27 dB), respectively. $PL_1 = 20.44\,\text{mm}$ achieves the lowest axial ratio (AR) for the band (7.9 GHz–8.4 GHz). Therefore, the selected value of PL_1 is 20.44 mm due to its largest bandwidth and lowest axial ratio (AR). The required bandwidth, circular polarization for the telemetry application, and size have not been achieved yet. In the upcoming step parametric study will be performed on PL_2 aiming to achieve the required bandwidth, circular polarization, and size.

TABLE 3. Dimensions of the three realization steps of the M-shaped polygonal slot antenna with embedded island.

	Step 1	Step 2	Step 2	Step 4
Parameter	**Value (mm)**	**Value (mm)**	**Value (mm)**	**Value (mm)**
PL_1	20.44	19.3	19.3	14.27
PL_2	8.84	11.03	11.03	7.7
PL_3	8.84	7.74	7.74	6.17
PL_4	8.84	7.74	7.74	10.8
PW_1	11.9	10.5	10.5	8.288
PW_2	6.08	5.3	5.3	4.24
PW	21.22	18.3	18.3	14.82
PL'_1	11.85	11.19	11.19	8.27
PL'_2	5.12	6.39	6.39	4.46
PL'_3	5.12	4.48	4.48	3.57
PL'_4	5.12	4.48	4.48	6.26
PW'_1	6.9	6.09	6.09	4.8
PW'_2	3.52	3.07	3.07	2.45
PW'	12.3	10.61	10.61	8.59
Sx	1.5	1.2	1.2	1.04
Sx_2	3.58	2.9	2.9	2.51
Sy	3.09	2.7	2.7	2.15
Sy_2	0.46	0.4	0.4	0.33
L_f	6.53	5.6	5.6	4.56
L_{tap}	6.2	5.3	5.3	4.36
W_f	1.53	1.53	1.53	1.53
W_{tap}	4.4	4.4	4.4	4.4
F_L	12	10.1	10.1	8.4
L	25.3	22.7	22.7	17
W	24.2	22.32	22.32	16

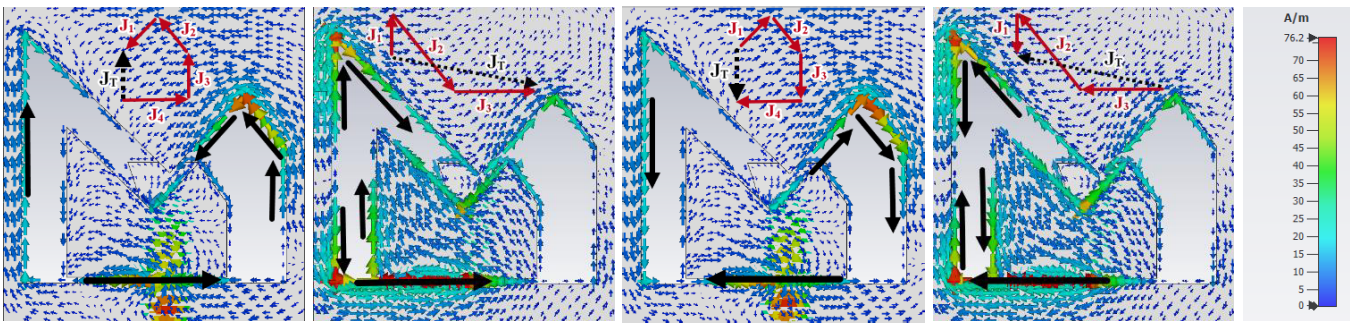

(a) (b) (c) (d)

FIGURE 20. Simulated surface current distribution at 8.15 GHz of the M-shaped polygonal slot antenna with embedded island at phase: (a) 0°, (b) 90°, (c) 180°, (d) 270°.

3.2. Step 2: Studying the Effect of Length PL_2

After selecting the value of PL_1 that achieves the largest bandwidth and lowest axial ratio (AR) as discussed in step 1. Step 2 takes place by performing a parametric study on PL_2. The slot antenna with the updated value of PL_1 is then simulated at different values of PL_2 while the other parameters are kept constant. The overall antenna size is reduced due to increasing the value of PL_2 which increased the effective length of the slot. Consequently, to maintain the same operating frequency band all the antenna dimensions are miniaturized. The overall antenna size ($L \times W$) is $22.7 \times 22.32\,\text{mm}^2$. The overall antenna size is reduced by 17.24% compared to step 1. The dimensions of the antenna at this step are given in Table 3. The reflection coefficient $|S_{11}|$ and the axial ratio curves at different values of PL_2 are shown in Figure 11 and Figure 12, respectively. It

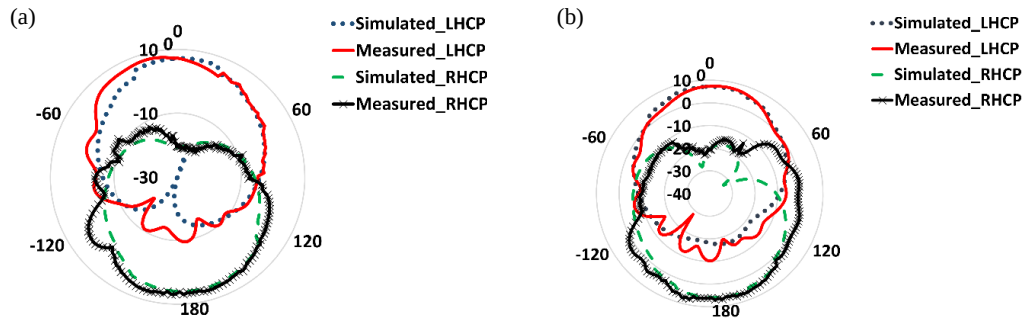

FIGURE 21. Measured vs simulated LHCP and RHCP, radiation patterns at 8.15 GHz: (a) E-plane (phi $= 0°$), (b) H-plane (phi $= 90°$).

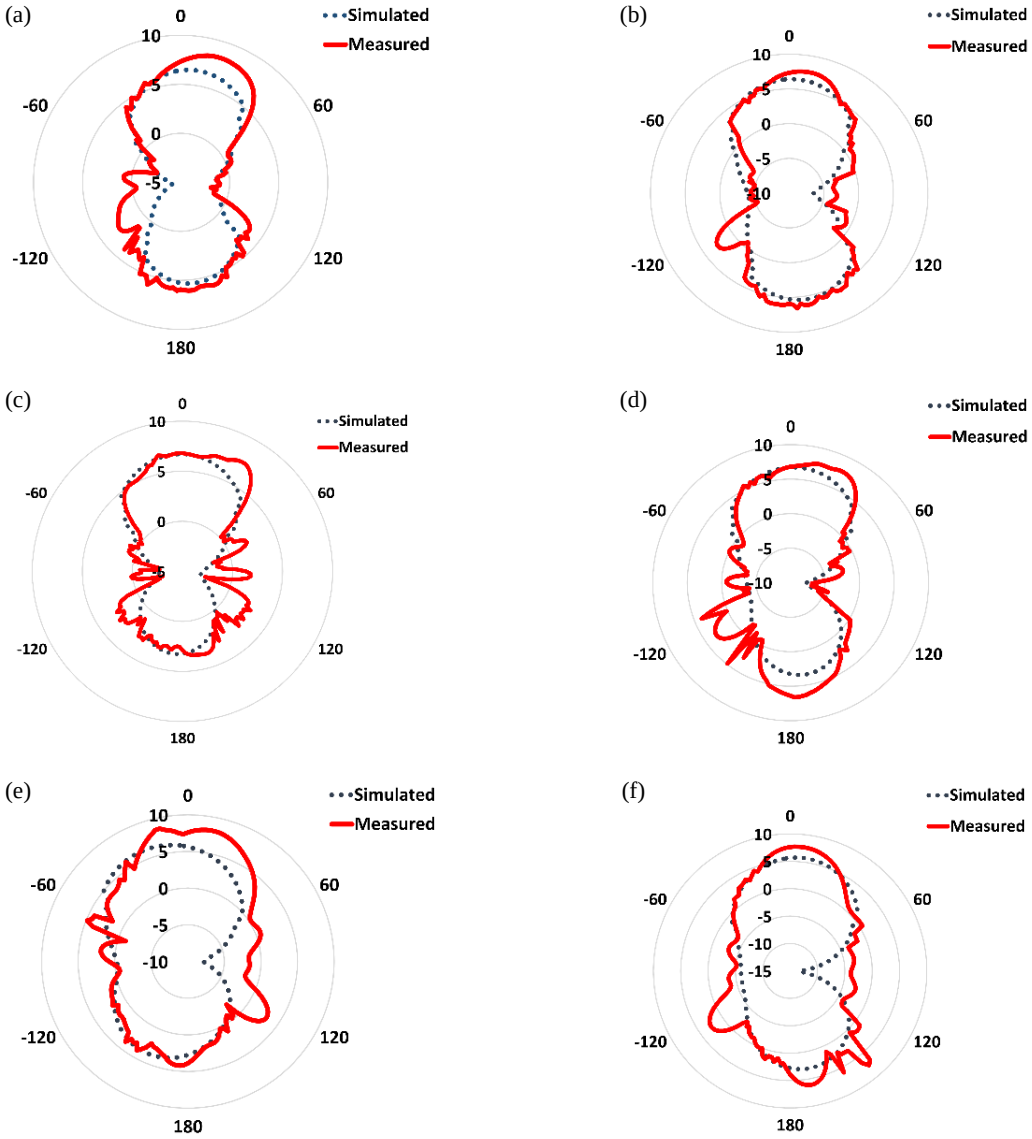

FIGURE 22. Measured vs simulated radiation pattern polar plot (theta vs dBi): (a) E-plane (phi $= 0°$) at 8.15 GHz, (b) H-plane (phi $= 90°$) at 8.15 GHz, (c) E-plane (phi $= 0°$) at 9 GHz, (d) H-plane (phi $= 90°$) at 9 GHz, (e) E-plane (phi $= 0°$) at 10 GHz, (f) H-plane (phi $= 90°$) at 10 GHz.

is shown in Figure 11 that the bandwidth at $PL_2 = 9.03$ mm, 11.03 mm, and 13.03 mm is 2.7 GHz, 3.1 GHz, and 2.4 GHz, respectively. $PL_2 = 11.03$ mm achieves the largest bandwidth with an improvement of 3.33% compared to step 1. It is shown in Figure 12 that the axial ratio (AR) in the band (7.9 GHz–8.4 GHz) for the three values of PL_2 exceeds 3 dB. The axial ratio for $PL_2 = 9.03$ mm, 11.03 mm, and 13.03 mm is in the range of (16.2 dB–17.8 dB), (15.5 dB–16 dB), and (14 dB–

14.5 dB), respectively. Therefore, the selected value of PL_2 is 11.03 mm due to its largest bandwidth and relatively low axial ratio (AR). The required bandwidth, circular polarization for the telemetry application, and size have not been achieved yet. In the upcoming step parametric study will be performed on PL_3 aiming to achieve the required bandwidth, circular polarization, and size.

3.3. Step 3: Studying the Effect of Length PL_3

After selecting the best value of PL_2 in terms of size, bandwidth, and circular polarization, step 3 takes place by performing a parametric study on PL_3. The slot antenna with the updated values of PL_1 and PL_2 is then simulated at different values of PL_3 while the other parameters are kept constant. The overall antenna size is not changed because the selected value of PL_3 remained 7.74 mm as it was in step 2. The dimensions of the antenna at this step are given in Table 3. The reflection coefficient $|S_{11}|$ and the axial Ratio curves at different values of PL_3 are shown in Figure 13 and Figure 14, respectively. It is shown in Figure 13 that the bandwidth at $PL_3 = 6.74$ mm, 7.74 mm, and 8.74 mm is 1.87 GHz, 2.56 GHz, and 1.93 GHz, respectively. $PL_3 = 7.74$ mm achieves the largest bandwidth, with no improvement compared to step 2. It is shown in Figure 14 that the axial ratio (AR) in the band (7.9 GHz–8.4 GHz) for the three values of PL_3 exceeds 3 dB. The axial ratio for $PL_2 = 6.74$ mm, 7.74 mm and 8.74 mm is in the range of (22 dB–23.5 dB), (15.5 dB–16 dB), and (36.5 dB–40 dB), respectively. $PL_3 = 7.74$ mm achieves the lowest axial ratio (AR) for the band (7.9 GHz–8.4 GHz). Therefore, the selected value of PL_3 is 7.74 mm due to its largest bandwidth and lowest axial ratio (AR). The required bandwidth, circular polarization for the telemetry application, and size have not been achieved yet. In the upcoming step parametric study will be performed on PL_4 aiming to achieve the required bandwidth, circular polarization, and size.

3.4. Step 4: Studying the Effect of Length PL_4

After selecting the best value of PL_3 in terms of size, bandwidth, and circular polarization, step 4 takes place by performing the parametric study on PL_4. The slot antenna with the updated values of PL_1, PL_2, and PL_3 is then simulated at different values of PL_4. The overall antenna size is reduced due to increasing the value of PL_4 which increased the effective length of the slot. Consequently, to maintain the same operating frequency band all the antenna dimensions are miniaturized. The overall antenna size $(L \times W)$ is $17 \times 16\,\text{mm}^2$. The overall antenna size is reduced by 46.3% compared to step 3. The dimensions of the antenna at this step are given in Table 3. The reflection coefficient $|S_{11}|$ and the axial ratio curves at different values of PL_4 are shown in Figure 15 and Figure 16, respectively. It is shown in Figure 15 that the bandwidth at $PL_4 = 8.8$ mm, 10.8 mm, and 12.8 mm is 2.1 GHz, 5.7 GHz, and 5 GHz, respectively. $PL_4 = 10.8$ mm achieves the largest bandwidth with an improvement of 83.9% compared to step 3, making the antenna suitable to operate for both the telemetry and SAR applications. It is shown in Figure 16 that the axial ratio (AR) at $PL_4 = 8.8$ mm, 10.8 mm, and 12.8 mm is below 3 dB in the bands (8.1 GHz–8.5 GHz), (7.8 GHz–8.55 GHz), and (7.73 GHz–8.25 GHz), respectively. $PL_1 = 20.44$ mm achieves the lowest axial ratio (AR) for the telemetry application band (7.9 GHz–8.4 GHz). $PL_4 = 10.8$ mm achieves the largest axial ratio (AR) bandwidth reaching 750 MHz and achieving circular polarization in the band (7.9 GHz–8.4 GHz). Therefore, the selected value of PL_4 is 10.8 mm due to its largest bandwidth and largest axial ratio (AR) bandwidth.

4. PROPOSED M-SHAPED POLYGONAL SLOT ANTENNA WITH EMBEDDED ISLAND

This section presents the final design of the proposed antenna, along with its simulated radiation patterns and antenna parameters. Additionally, the fabricated prototype of the antenna is introduced, including the measured radiation patterns and antenna parameters. Figure 17 shows the final form of the M-shaped polygonal slot antenna with the embedded island. The final structure of the antenna has slot dimensions of (PL_1, PL_2, PL_3, PL_4, PW_1 and PW_2) that achieve the required results. The dimensions are given in Table 3. The proposed M-shaped polygonal slot antenna with the embedded island was fabricated using an RT/Duroid 5880 substrate with dielectric constant, $\varepsilon_r = 2.2$, low loss tangent $\tan(\delta) = 0.0009$, and height $h = 0.508$ mm. Figures 18(a) and (b) show photographs of the fabricated M-shaped polygonal slot antenna with the embedded island front view and back view. The reflection coefficient $|S_{11}|$ of the M-shaped polygonal slot antenna with the embedded island is measured using Rohde & Schwarz Vector Network Analyzer (VNA). The radiation pattern and other antenna parameters were then measured in a SATEMO Anechoic Chamber as shown in Figure 19. To justify the circular polarization property mechanism, Figure 20 shows the simulated surface current at 8.15 GHz. The surface current distribution of an antenna is an important parameter that determines its radiation characteristics. Figures 20(a), (b), (c), and (d) are provided to describe the surface current distributions at phase angles of 0, 90, 180, and 270 degrees, respectively with maximum surface current of 76.2 A/m. The total surface current, J_T, represents the vector summation of all the significant surface current distributions at each phase. It is observed that the total surface current, J_T, at 0 and 90 degrees are equal in magnitude and opposite in direction to that at 180 and 270 degrees. It can be observed that the total surface current, J_T, direction is rotating clockwise when comparing each phase to the previous one, and accordingly a left-hand circularly polarized (LHCP) radiation is generated in the positive z direction (antenna front side). The proposed antenna can excite LHCP and RHCP waves [27, 28]. The proposed antenna is a bidirectional simultaneous dual circularly polarized antenna, as it is able to generate a left-hand circular polarization (LHCP) in the positive z direction (antenna front side), whereas a right-hand circular polarization (RHCP) is generated in the negative z direction (antenna back side) at the same time [27, 28]. The simulated and measured LHCP and RHCP radiation patterns at 8.15 GHz are shown in Figure 21. The simulated and measured radiation patterns and antenna parameters of the polygonal M-shaped slot antenna are analyzed and compared. The radiation patterns E-

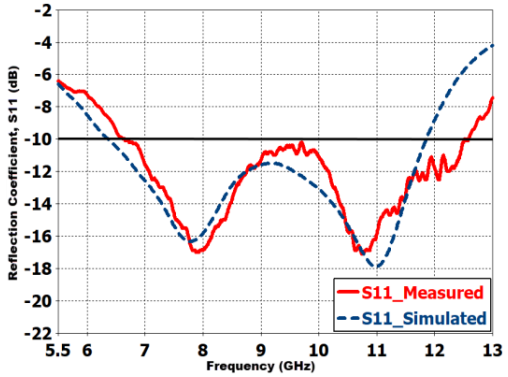

FIGURE 23. Measured vs simulated reflection coefficient $|S_{11}|$ of the M-shaped polygonal slot antenna with embedded island.

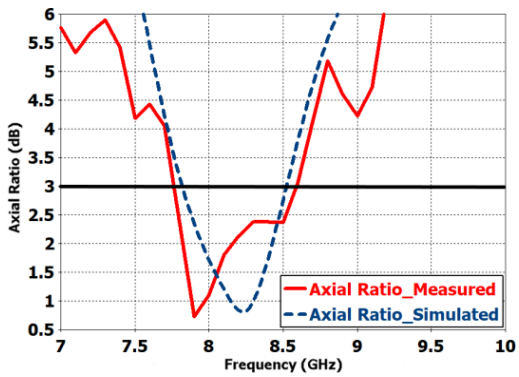

FIGURE 24. Measured vs simulated Axial Ratio (AR) of the M-shaped polygonal slot antenna with embedded island.

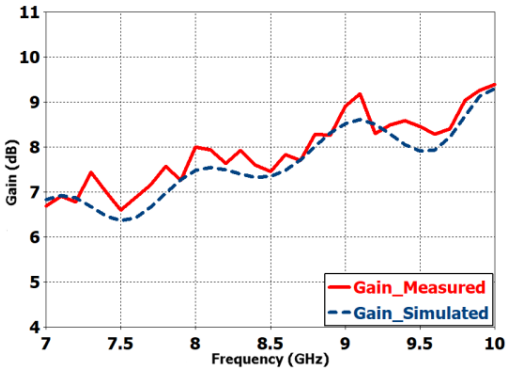

FIGURE 25. Measured vs simulated gain of the M-shaped polygonal slot antenna with embedded island.

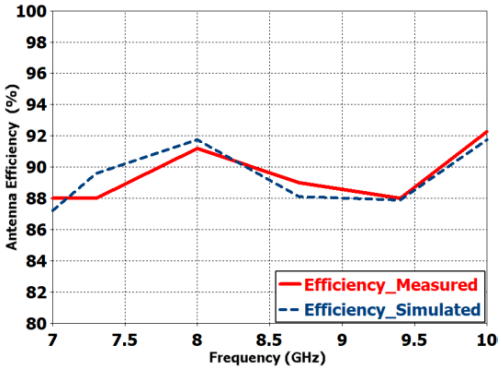

FIGURE 26. Measured vs simulated antenna efficiency of the M-shaped polygonal slot antenna with embedded island.

TABLE 4. Comparison with some recent designs of X-band antennas.

Reference	Bandwidth (Hz)	Axial Ratio 3 dB Bandwidth (Hz)	Dual Circular Polarization	Maximum Gain (dBi)	Antenna Size (mm^3)
[1]	8.025–8.4 GHz (370 MHz)	8.025–8.4 GHz (370 MHz)	Yes	5 dBi	Diameter: 238 mm ($6.52\lambda_0$) Height: 185 mm ($5.13\lambda_0$)
[2]	8–9.7 GHz (1.7 GHz)	8.3–8.88 GHz (580 MHz)	No	14 dBi	(Length × Width × Height): 62 mm × 62 mm × 22 mm ($1.77\lambda_0 \times 1.77\lambda_0 \times 0.63\lambda_0$)
[3]	8–8.4 GHz (400 MHz)	8–8.4 GHz (400 MHz)	No	5 dBi	(Length × Width × Height): 100 mm × 100 mm × 15 mm ($2.74\lambda_0 \times 2.74\lambda_0 \times 0.41\lambda_0$)
[4]	9.4–10.5 GHz (1.1 GHz)	Not Circularly Polarized	No	9 dBi	(Length × Width × Height): 59 mm × 14 mm × 0.76 mm ($1.96\lambda_0 \times 0.46\lambda_0 \times 0.025\lambda_0$)
[5]	9.01-10.2 GHz (1.19 GHz)	Not Circularly Polarized	No	8 dBi	(Length × Width × Height): 14 mm × 14 mm × 3.986 mm ($0.45\lambda_0 \times 0.45\lambda_0 \times 0.126\lambda_0$)
This work	6.63–12.566 GHz (5.936 GHz)	7.76–8.58 GHz (820 MHz)	Yes	9.4 dBi	(Length × Width × Height): 17 mm × 16 mm × 0.508 mm ($0.56\lambda_0 \times 0.53\lambda_0 \times 0.016\lambda_0$)

plane (phi $= 0°$) and H-plane (phi $= 90°$) at frequencies of 8.15 GHz, 9 GHz and 10 GHz for the simulated and fabricated antennas are shown in Figures 22(a), (b), (c), (d), (e), and (f), respectively. The simulated and measured reflection coeffi-

cients $|S_{11}|$ are shown in Figure 23 with -10 dB bandwidths of 5.5 GHz extending from 6.3 GHz to 12 GHz and 6.1 GHz extending from 6.5 GHz to 12.6, respectively. The simulated and measured axial ratios (ARs) are shown in Figure 24 indicating that the antenna is circularly polarized in the required band. The simulated and measured AR 3-dB bandwidths are 750 MHz (extending 7.8 GHz to 8.55 GHz) and 820 MHz (extending from 7.76 GHz to 8.58 GHz), respectively. The simulated and measured gains are shown in Figure 25 with maximum gains of 9.3 dBi and 9.4 dBi, respectively. The simulated and measured total efficiencies are shown in Figure 26 with maximum efficiencies of 92% and 92.2%, respectively. This indicates that the proposed antenna design is well optimized and capable of achieving excellent performance in terms of efficient use of the available power. The results demonstrate that the measured parameters and radiation patterns of the fabricated antenna match the simulation results, achieving the desired design requirements.

5. FINAL ASSESSMENT AND COMPARISON WITH RECENT X-BAND ANTENNA DESIGNS

This section presents a comprehensive comparison of the proposed "M-shaped polygonal slot antenna with embedded island" with several recent X-band antenna designs as given in Table 4. The proposed design exhibits remarkable performance in terms of bandwidth, small size, and circular polarization in the required band. The table provides a detailed comparison of different antenna designs in terms of bandwidth, axial ratio 3-dB bandwidth, maximum gain, and antenna size. It is evident that the proposed design outperforms other designs in terms of bandwidth, with a bandwidth of 5.97 GHz extending from 6.63 GHz to 12.566 GHz, which is exceptionally wide compared to the other designs. Moreover, the proposed design achieves simultaneous dual circular polarizations (LHCP and RHCP) in the required band for X-band telemetry application. The proposed antenna is suitable for both satellite telemetry application and synthetic aperture radar (SAR) on small satellites application. The proposed design also demonstrates a small size with dimensions of 17 mm $\times$ 16 mm $\times$ 0.508 mm ($0.56\lambda_0 \times 0.53\lambda_0 \times 0.016\lambda_0$), which is significantly smaller than most of the other designs while still achieving a high maximum gain of 9.4 dBi. The results of this study demonstrate that the proposed X-band antenna design offers superior performance compared to existing designs.

6. CONCLUSION

In this paper, an M-shaped polygonal slot antenna with embedded island is designed, simulated, fabricated, and tested. The method for achieving the M-shaped polygonal slot from the rectangular slot for size, bandwidth, and axial ratio (AR) enhancement is introduced and illustrated. The antenna achieved a bandwidth of 5.97 GHz covering the whole X-band from 6.63 GHz to 12.566 GHz. The antenna is circularly polarized with a simultaneous dual circular polarizations (RHCP and LHCP). The realized axial ratio (AR) 3 dB bandwidth is 820 MHz from 7.76 GHz to 8.58 GHz. The proposed antenna is suitable for both satellite telemetry application and Synthetic Aperture Radar (SAR) on small satellites application. The maximum achieved antenna gain is equal to 9.4 dBi. The final overall antenna size is small with dimensions $17 \times 16 \times 0.508\,\text{mm}^3$. The proposed antenna design exhibits a remarkably large gain relative to its small size, demonstrating the effectiveness of the design in terms of compactness and efficiency. The total antenna efficiency reaches 92%. This suggests that the proposed antenna design is well tuned and can accomplish an outstanding performance. The performance of the proposed design approach has been evaluated through measurements taken on a prototype that was fabricated, and the results have demonstrated that the approach is reliable.

REFERENCES

[1] Arnaud, E., J. Dugenet, K. Elis, A. Girardot, D. Guihard, C. Menudier, T. Monediere, F. Roziere, and M. Thevenot, "Compact isoflux X-band payload telemetry antenna with simultaneous dual circular polarization for LEO satellite applications," *IEEE Antennas and Wireless Propagation Letters*, Vol. 19, No. 10, 1679–1683, Oct. 2020.

[2] Leszkowska, L., M. Rzymowski, K. Nyka, and L. Kulas, "High-gain compact circularly polarized X-band superstrate antenna for cubesat applications," *IEEE Antennas and Wireless Propagation Letters*, Vol. 20, No. 11, 2090–2094, Nov. 2021.

[3] Fouany, J., M. Thevenot, E. Arnaud, F. Torres, C. Menudier, T. Monediere, and K. Elis, "New concept of telemetry X-band circularly polarized antenna payload for cubesat," *IEEE Antennas and Wireless Propagation Letters*, Vol. 16, 2987–2991, 2017.

[4] El Khamlichi, D., N. Amar Touhami, T. Elhamadi, and M. Ali Ennasar, "High-gain and broadband SIW cavity-backed slots antenna for X-band applications," *International Journal of Microwave and Wireless Technologies*, Vol. 13, No. 10, 1078–1085, Dec. 2021.

[5] Anim, K., P. Danuor, S.-O. Park, and Y.-B. Jung, "High-efficiency broadband planar array antenna with suspended microstrip slab for X-band SAR onboard small satellites," *Sensors*, Vol. 22, No. 1, Jan. 2022.

[6] Çelenk, E. and N. T. Tokan, "All-textile on-body antenna for military applications," *IEEE Antennas and Wireless Propagation Letters*, Vol. 21, No. 5, 1065–1069, May 2022.

[7] Preradovic, S. and A. Menicanin, "X-band semi-passive RFID tag on flexible laminate," in *2012 42nd European Microwave Conference (EUMC)*, 892–895, Amsterdam, Netherlands, Oct.-Nov. 2012.

[8] Adhitya, G., V. Abishek, R. Mohana Sundaram, and P. Jothilakshmi, "Design of microstrip antenna for X band satellite communications," *International Journal of Research and Analytical Reviews (IJRAR)*, Vol. 6, No. 2, 342–344, May 2019.

[9] Imbraile, W., S. Gao, and L. Boccia, *Space Antenna Handbook*, Wiley, New Jersey, 2012.

[10] Khac, K. N., N. D. Phong, L. H. Manh, T. A. L. Trong, and D. N. Chien, "A design of circularly polarized array antenna for X-band CubeSat satellite communication," in *2018 International Conference on Advanced Technologies For Communications (ATC)*, Ho Chi Minh City, Vietnam, 2018.

[11] Aliqab, K., S. Lavadiya, M. Alsharari, A. Armghan, M. G. Daher, and S. K. Patel, "Design and fabrication of a low-cost, multiband and high gain square tooth-enabled metamaterial superstrate microstrip patch antenna," *Micromachines*, Vol. 14, No. 1, Jan. 2023.

[12] Genovesi, S. and F. A. Dicandia, "Characteristic modes analysis of a near-field polarization-conversion metasurface for the design of a wideband circularly polarized X-band antenna," *IEEE Access*, Vol. 10, 88 932–88 940, 2022.

[13] Yadav, M. V., S. Buadha, and S. C. Singam, "Multiple slot planar antenna for X-band satellite mobile communication," *IEEE 7th Uttar Pradesh Section International Conference on Electrical, Electronics and Computer Engineering (UPCON)*, 2020.

[14] Karmakar, A., "Fractal antennas and arrays: A review and recent developments," *International Journal of Microwave and Wireless Technologies*, Vol. 13, No. 2, 173–197, Mar. 2021.

[15] Ellis, M. S., F. B. Effah, A.-R. Ahmed, J. J. Kponyo, J. Nourinia, C. Ghobadi, and B. Mohammadi, "Asymmetric circularly polarized open-slot antenna," *International Journal of RF and Microwave Computer-aided Engineering*, Vol. 30, No. 5, May 2020.

[16] Chen, Q., H. Zhang, L.-C. Yang, H.-P. Li, T. Zhong, X.-L. Min, and S.-L. Tan, "Novel dual-band asymmetric U-shaped slot antenna for dual-circular polarization," *International Journal of RF and Microwave Computer-Aided Engineering*, Vol. 27, No. 1, Jan. 2017.

[17] Sun, X.-B., M.-Y. Cao, J.-J. Hao, and Y.-J. Guo, "A rectangular slot antenna with improved bandwidth," *AEU-International Journal of Electronics and Communications*, Vol. 66, No. 6, 465–466, 2012.

[18] Moitra, S. and A. K. Mukhopadhyay, "Ku-band substrate integrated waveguide (SIW) slot array antenna for next generation networks," *Global Journal of Computer Science & Technology*, No. 5, 2013.

[19] Balanis, C. A., *Antenna Theory: Analysis and Design*, 4th Edition, Wiley, New York, United States, 2016.

[20] Hassan, M. H., B. Sievert, A. Rennings, and D. Erni, "Generation of vortex waves using crossed 2λ-dipole antennas," in *2021 15th European Conference on Antennas and Propagation (EUCAP)*, Dusseldorf, Germany, Mar. 2021.

[21] Anantrasirichai, N., S. Chanoodhorm, J. Nakasuwan, P. Rakluea, and T. Wakabayashi, "Designing rectangular slot loop antenna for WLAN application," in *Tencon 2005 — 2005 IEEE Region 10 Conference*, Vols. 1–5, Melbourne, Australia, Nov. 2006.

[22] Trinh-Van, S., Y. Yang, K.-Y. Lee, Y. S. Kim, and K. C. Hwang, "Bandwidth-enhanced circularly polarized crescent-shaped slot antenna via circular-patch loading," *Applied Sciences*, Vol. 9, No. 6, 1117–1126, Mar. 2019.

[23] Kumar, B., B. K. Shukla, A. Somkuwar, and O. P. Meena, "Analysis of hexagonal wide slot antenna with parasitic element for wireless application," *Progress In Electromagnetics Research C*, Vol. 94, 145–159, 2019.

[24] Abed, A. T., M. S. J. Singh, and A. M. Jawad, "Investigation of circular polarization technique in Q-slot antenna," *International Journal of Microwave and Wireless Technologies*, Vol. 12, No. 2, 176–182, Mar. 2020.

[25] Kwon, O. H., W. B. Park, S. Lee, J. M. Lee, Y. M. Park, and K. C. Hwang, "3D-printed super-wideband spidron fractal cube antenna with laminated copper," *Applied Sciences*, Vol. 7, No. 10, 1–9, Oct. 2017.

[26] Elsebai, M., T. M. Abdelfadl, and F. Ibrahim, "Frequency transformation to design single band rectangular patch mmw antennas," in *2017 Progress In Electromagnetics Research Symposium — Spring (PIERS)*, 203–210, St Petersburg, Russia, May 2017.

[27] Huang, T., G.-B. Liu, H.-F. Zhang, and L. Zeng, "A new adjustable frequency waveguide circularly polarized antenna based on the solid-state plasma," *Applied Physics A — Materials Science & Processing*, Vol. 125, No. 9, 659–660, Sep. 2019.

[28] Mohammadi, S., J. Nourinia, C. Ghobadi, J. Pourahmadazar, and M. Shokri, "Compact broadband circularly polarized slot antenna using two linked elliptical slots for C-band applications," *IEEE Antennas and Wireless Propagation Letters*, Vol. 12, 1094–1097, 2013.